



Diamagnetism and density-wave order in the pseudogap regime of $\text{YBa}_2\text{Cu}_3\text{O}_{6+x}$

Citation

Hayward, Lauren E., Andrew J. Achkar, David G. Hawthorn, Roger G. Melko, and Subir Sachdev. 2014. "Diamagnetism and Density-Wave Order in the Pseudogap Regime of $\text{YBa}_2\text{Cu}_3\text{O}_{6+x}$." Phys. Rev. B 90 (9) (September). doi:10.1103/physrevb.90.094515.

Published Version

doi:10.1103/PhysRevB.90.094515

Permanent link

<http://nrs.harvard.edu/urn-3:HUL.InstRepos:16380263>

Terms of Use

This article was downloaded from Harvard University's DASH repository, and is made available under the terms and conditions applicable to Open Access Policy Articles, as set forth at <http://nrs.harvard.edu/urn-3:HUL.InstRepos:dash.current.terms-of-use#OAP>

Share Your Story

The Harvard community has made this article openly available.
Please share how this access benefits you. [Submit a story](#).

[Accessibility](#)

Diamagnetism and density wave order in the pseudogap regime of $\text{YBa}_2\text{Cu}_3\text{O}_{6+x}$

Lauren E. Hayward,¹ Andrew J. Achkar,¹ David G. Hawthorn,¹ Roger G. Melko,^{1,2} and Subir Sachdev^{3,2}

¹*Department of Physics and Astronomy, University of Waterloo, Ontario, N2L 3G1, Canada*

²*Perimeter Institute for Theoretical Physics, Waterloo, Ontario N2L 2Y5, Canada*

³*Department of Physics, Harvard University, Cambridge, MA 02138, USA*

(Dated: June 12, 2014)

Clear experimental evidence of charge density wave correlations competing with superconducting order in YBCO have thrust their relationship with the pseudogap regime into the spotlight. To aid in characterizing the pseudogap regime, we propose a dimensionless ratio of the diamagnetic susceptibility to the correlation length of the charge density wave correlations. Using Monte Carlo simulations, we compute this ratio on the classical model of Hayward *et al.* (Science **343**, 1336 (2014)), which describes angular fluctuations of a multicomponent order, capturing both superconducting and density wave correlations. We compare our results with available data on $\text{YBa}_2\text{Cu}_3\text{O}_{6+x}$, and propose experiments to clarify the value of this dimensionless ratio using existing samples and techniques.

I. INTRODUCTION

A fundamental characteristic of the pseudogap regime of the hole-doped cuprate superconductors has been the presence of a large diamagnetic susceptibility over a wide range of temperatures above the critical temperature for superconductivity.^{1–4} This behavior has been modeled in various theories of thermal fluctuations of the superconducting order and its vortices.^{5–8}

On the other hand, a seemingly different view of the pseudogap has emerged from recent X-ray scattering experiments.^{9–15} In a regime of doping where the anti-ferromagnetic correlations are weak, these experiments observe substantial charge density wave (CDW) correlations. The temperature and magnetic field dependence of these observations indicate that the CDW order competes with the superconducting (SC) order.

It is the purpose of the present paper to reconcile these distinct experimental probes of the pseudogap. First, one can measure the strength of the SC fluctuations by the diamagnetic susceptibility, $\chi_d = M/B$, where M is the magnetization per unit volume in the presence of a field B applied perpendicular to the CuO_2 layers. Second, one can characterize the CDW correlations by the value of their correlation length ξ_{cdw} . From these quantities, which can be directly measured in experiments on the same sample in absolute units, we propose to form the following dimensionless ratio:

$$R(T) = 12\pi s \left(\frac{\hbar}{2e} \right)^2 \frac{\chi_d}{k_B T \xi_{\text{cdw}}^2}. \quad (1)$$

Here e is the electron charge, s is the interlayer spacing, T is the absolute temperature, and the prefactor of 12π is for numerical convenience.

The utility of $R(T)$ extends to both experiment and theory. It is directly measurable from magnetic susceptibility and X-ray scattering experiments (preferably from the same sample), and offers a dimensionless mea-

sure of the relative strength of the fluctuations of the order parameters for superconductivity and charge density waves. Previous models of diamagnetism^{5–8} have used phenomenological theories for superconducting fluctuations with a number of adjustable parameters. Our model has a similar effective theory for superconductivity, but the *same* parameters *also* determine the charge order fluctuations. By taking a dimensionless ratio, the theoretical predictions become insensitive to the short-distance cutoff of the theory, and to the arbitrary scales used in defining the order parameters. Measurements and computations of $R(T)$ therefore offer a route to comparing our understanding of the pseudogap to a more constrained theory.

Experimentally, indications of a close relationship between superconductivity and the CDW order appeared already in the classic scanning tunneling microscopy observations of Hoffman *et al.*¹⁶ These experiments observed a CDW ‘halo’ about each vortex in the superconducting order. In the pseudogap regime, the thermal fluctuations of vortex-antivortex pairs are clearly the key to the diamagnetic response, as in the models of Refs. 6–8; however these works considered only ‘naked’ vortices in the superconducting order, whose core did not possess any CDW correlations. Here we shall employ our recently proposed model of the pseudogap in Ref. 17, in which the superconducting vortices are indeed linked to CDW correlations: this is captured by a snapshot from our Monte Carlo simulations in Fig. 1. Thus, in our model, the vortex fluctuations involved in the diamagnetic response, are also directly tied to X-ray measurements of CDW correlations. We can, therefore, view $R(T)$ as a quantitative measure of the remarkable link between the seemingly disparate superconducting and CDW orders.

Our model¹⁷ characterizes the CDW and SC fluctuations by a composite order parameter with six real components, and focuses on classical and thermal fluctuations of this order along the angular directions of the 6-dimensional space. In Ref. 17, the parameters of the

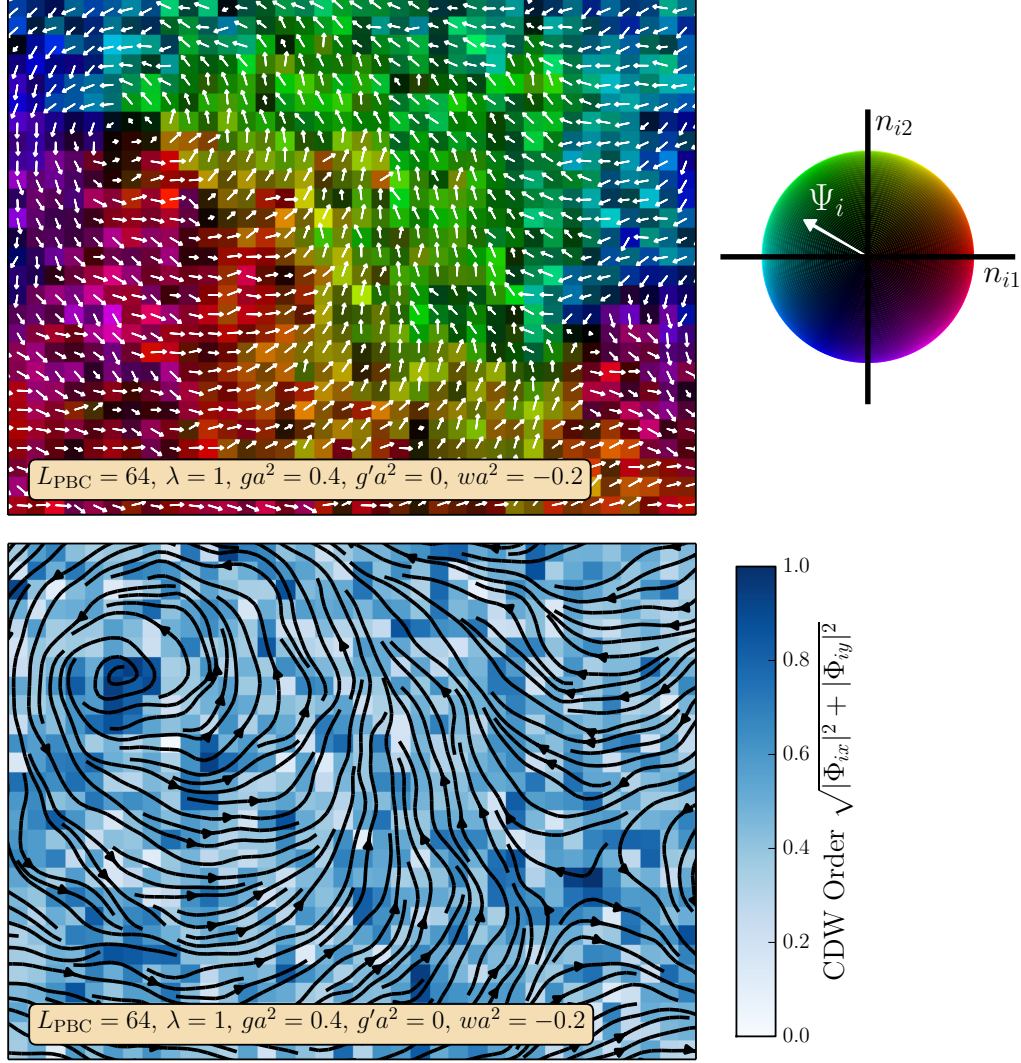


FIG. 1. Sample system configuration of the model of Ref. 17 when $T/\rho_s = 0.18$ (below the Kosterlitz-Thouless transition). We show a configuration of the variables $n_{i\alpha}$ on a subregion of a 64×64 lattice. We use a representative set of model parameters and employ two different visualization techniques. In the upper plot, we use shading to represent the strength of the CDW order parameter, with darker shading corresponding to stronger CDW magnitude $\sqrt{|\Phi_{ix}|^2 + |\Phi_{iy}|^2}$ on site i , and color to represent the orientation of the variables in the SC plane. The white arrows here correspond to the magnitude and orientation of the SC order Ψ_i . The lower plot uses color to represent the magnitude of the CDW order parameter and black arrows to illustrate the streamlines of Ψ_i . In both plots, a vortex-antivortex pair is visible in the upper left and lower right corners. The enhancement of CDW correlations in the vicinities of these vortices is also visible.

energy functional in the thermal partition function were constrained by comparing to X-ray data,¹⁷ which reflected the strong coupling between the SC and CDW order parameters. Here, we present our results for $R(T)$ for a similar range of parameters. We compare these computations with the available data on $\text{YBa}_2\text{Cu}_3\text{O}_{6+x}$, although the present diamagnetic susceptibility and X-ray data are not on the same sample. Despite these caveats, we show below that the absolute theoretical and experimental values of $R(T)$ are quite close to each other, and their T -dependencies are very similar. We hope that our

theoretical calculations will motivate experimental measurements of $R(T)$ on a single sample in the near future.

II. THEORETICAL MODEL AND MEASUREMENTS

The model of Ref. 17 describes the pseudogap using a non-linear sigma model (NL σ M) with classical variables $n_{i\alpha}$ ($\alpha = 1 \dots 6$) on sites i of a square lattice, with the constraint $\sum_{\alpha} n_{i\alpha}^2 = 1$ on every site i . These variables

describe the SC order Ψ , the CDW order Φ_x along the x direction, and the CDW order Φ_y along the y direction via

$$\begin{aligned}\Psi &= n_1 + in_2 \\ \Phi_x &= n_3 + in_4 \\ \Phi_y &= n_5 + in_6.\end{aligned}\quad (2)$$

The partition function, \mathcal{Z} , of the NL σ M is given by

$$\mathcal{Z} = \prod_i \left[\int dn_{i\alpha} \delta\left(\sum_{\alpha=1}^6 n_{i\alpha}^2 - 1\right) \right] \exp\left(-\frac{H_1 + H_2}{k_B T}\right), \quad (3)$$

where

$$\begin{aligned}H_1 &= \frac{\rho_s}{2} \sum_{\langle ij \rangle} \left[\sum_{\alpha=1}^2 (n_{i\alpha} - n_{j\alpha})^2 + \lambda \sum_{\alpha=3}^6 (n_{i\alpha} - n_{j\alpha})^2 \right], \\ H_2 &= \rho_s a^2 \sum_i \left[\frac{g}{2} \sum_{\alpha=3}^6 n_{i\alpha}^2 + \frac{g'}{2} \left(\sum_{\alpha=3}^6 n_{i\alpha}^2 \right)^2 \right. \\ &\quad \left. + \frac{w}{2} [(n_{i3}^2 + n_{i4}^2)^2 + (n_{i5}^2 + n_{i6}^2)^2] \right].\end{aligned}\quad (4)$$

The couplings ρ_s and $\rho_s \lambda$ are the helicity moduli for spatial variations of the SC and CDW orders, and g measures the anisotropy in the energy between the CDW and SC directions. We also allow here for a quartic anisotropy g' , which was not included in Ref. 17, in order to obtain a wider range of physical properties. The continuum theory is discretized on a lattice of spacing a . The lattice spacing a will cancel out of our computations for the value of $R(T)$.

The ground state of \mathcal{Z} at $T = 0$ is easily determined: the optimal state is spatially uniform with $H_1 = 0$, and we have to minimize H_2 . Let us first take $w < 0$ so that the CDW is stripe-like *i.e.* only one of Φ_x or Φ_y is non-zero. Then, without loss of generality we can take

$$n_\alpha = (\cos \theta, 0, \sin \theta, 0, 0, 0), \quad (5)$$

where $\theta = 0$ corresponds to SC order, $\theta = \pi/2$ corresponds to CDW order, and anything in between is co-existence, namely SC+CDW. Then, per site,

$$\frac{H_2}{\rho_s a^2} = \frac{g}{2} \sin^2 \theta + \frac{w + g'}{2} \sin^4 \theta. \quad (6)$$

Minimizing this function gives the parameter-dependent ground state

$$\begin{aligned}\text{SC} &: g > 0, \quad w + g' + g > 0 \\ \text{CDW} &: g > 0, \quad w + g' + g < 0 \\ \text{CDW} &: g < 0, \quad w + g' + g/2 < 0 \\ \text{SC + CDW} &: g < 0, \quad w + g' + g/2 > 0.\end{aligned}\quad (7)$$

Next, we consider $w > 0$ so that the CDW is ‘checker-board’. Then, without loss of generality we can take

$$n_\alpha = \left(\cos \theta, 0, \frac{\sin \theta}{\sqrt{2}}, 0, \frac{\sin \theta}{\sqrt{2}}, 0 \right), \quad (8)$$

and then

$$\frac{H_2}{\rho_s a^2} = \frac{g}{2} \sin^2 \theta + \frac{w/2 + g'}{2} \sin^4 \theta, \quad (9)$$

so that the minima are as in Eq. (7), but with $w \rightarrow w/2$.

At finite temperature, an exact solution to the model is unavailable, and we turn to a numerical solution based on Monte Carlo simulations as described in the next section. There, we focus on using the dimensionless ratio $R(T)$ to characterize the various phases of the model, for which one requires calculation of the susceptibility and correlation length. We now describe the general method for computing the magnetization, M , of \mathcal{Z} in the presence of an applied magnetic field. We access M on a $L \times L$ lattice with open boundary conditions using the method of Ref. 18, which allows us to avoid introducing flux quantization, which therefore means that we can consider the effect of arbitrarily small magnetic fields B (in contrast, for example, to the cylindrical boundary conditions used in Refs. 7 and 8). The expression for the magnetization can be computed by introducing an external vector potential \mathbf{A} . We assume that there is only an orbital coupling to the superconducting order, $\Psi_j = n_{j1} + in_{j2}$. The contribution to the kinetic part from this coupling between Ψ and \mathbf{A} is then written as

$$\begin{aligned}H_\Psi &= H_1 \Big|_\Psi \\ &= \frac{\rho_s}{2} \sum_{\langle ij \rangle} \left(|\Psi_i|^2 + |\Psi_j|^2 - \Psi_i^* \Psi_j e^{iA_{ij}} - \Psi_j^* \Psi_i e^{-iA_{ij}} \right),\end{aligned}\quad (10)$$

where

$$A_{ij} = \frac{2e}{\hbar} \int_{\mathbf{r}_i}^{\mathbf{r}_j} d\mathbf{r} \cdot \mathbf{A}. \quad (11)$$

We will henceforth drop factors of $2e$ and \hbar . We take L even and place the origin of co-ordinates at the center of the central plaquette. Thus, the sites are at

$$\mathbf{r}_i \equiv (x_i, y_i) = \left(i_x - \frac{L+1}{2}, i_y - \frac{L+1}{2} \right) a, \quad (12)$$

with $i_{x,y} = 1 \dots L$. It is now convenient to label the site-dependence of the vector potential as A_{iu} , where \mathbf{u} extends over $\pm \hat{x}a$ and $\pm \hat{y}a$ for bulk sites, and a smaller range for sites on the edge. Then we can write H_Ψ as

$$\begin{aligned}H_\Psi &= \frac{\rho_s}{2} \sum_i Z_i |\Psi_i|^2 - \frac{\rho_s}{2} \sum_{i,u} \Psi_i^* \Psi_{i+u} e^{iA_{iu}} \\ &= \frac{\rho_s}{2} \sum_i Z_i |\Psi_i|^2 - \frac{\rho_s}{2} \sum_{i,u} \Psi_{i+u}^* \Psi_i e^{-iA_{iu}},\end{aligned}\quad (13)$$

where Z_i is the co-ordination number for site i . Thus the sum over u always extends over Z_i values. Note that $A_{i+u,-u} = -A_{iu}$. The current flowing along link iu is then

$$\mathbf{J}_{iu} = \mathbf{u} \frac{\rho_s}{2} (i\Psi_i^* \Psi_{i+u} e^{iA_{iu}} + \text{c.c.}). \quad (14)$$

Finally, following Ref. 18, we can write the total magnetic moment divided by the volume as

$$\begin{aligned} M &= \frac{1}{4L^2 a^2 s} \sum_{i,u} \mathbf{r}_i \times \langle \mathbf{J}_{iu} \rangle \\ &= \frac{\rho_s}{4L^2 a^2 s} \sum_{i,u} \epsilon_{\alpha\beta} r_{i\alpha} u_\beta \langle i\Psi_i^* \Psi_{i+u} e^{iA_{iu}} \rangle. \end{aligned} \quad (15)$$

We apply a uniform magnetic field B perpendicular to the plane, and choose the vector potential in the circular gauge

$$A_{iu} = \frac{B}{2} \epsilon_{\alpha\beta} r_{i\alpha} u_\beta. \quad (16)$$

Now we expand M to first order in B and obtain

$$\begin{aligned} \chi_d \equiv \frac{M}{B} &= -\frac{\rho_s}{8L^2 a^2 s} \sum_{i,u} (\epsilon_{\alpha\beta} r_{i\alpha} u_\beta)^2 \langle \Psi_i^* \Psi_{i+u} \rangle_0 \\ &+ \frac{\rho_s^2}{16TL^2 a^2 s} \sum_{i,u} \sum_{j,u'} (\epsilon_{\alpha\beta} r_{i\alpha} u_\beta) (\epsilon_{\gamma\delta} r_{j\gamma} u'_\delta) \\ &\times \langle \Psi_i^* \Psi_{i+u} \Psi_{j+u'}^* \Psi_j \rangle_0, \end{aligned} \quad (17)$$

where the subscript 0 indicates that the averages can be evaluated in zero field under \mathcal{Z} . Note that the expression (17) is proportional to a^2 (after accounting for the powers of a in \mathbf{r}_i and \mathbf{u}_i); this factor of a^2 will cancel with that in ξ_{cdw} when we compute the ratio $R(T)$.

As described in the next section, we use this expression for χ_d to calculate the linear-order diamagnetic susceptibility of the model of Eq. (3). However, before proceeding with the full NL σ M, we carefully benchmark our expression for M/B by calculating it for a simple Gaussian model, where exact analytical results are available. As described in Appendix A, we find excellent agreement between our Monte Carlo results and Feynman diagram computations for this Gaussian model.

III. MONTE CARLO SIMULATION

By using classical Monte Carlo techniques, one can solve for thermodynamic properties of the model of Ref. 17, i.e., Eq. (3), on a finite-size lattice. These techniques involve importance-sampling of configurations of the classical variables $n_{i\alpha}$ according to a Boltzmann probability distribution. In order to generate independent configurations weighted by the partition function \mathcal{Z} , we use a combination of local^{19–21} and non-local^{21,22} sampling techniques. Both of these sampling techniques

require a method for generating a random point (corresponding to the coordinates $n_{i\alpha}$) on a hypersphere in 6-dimensional space. In order to generate such a random point, we choose each of the coordinates $n_{i\alpha}$ from a normal distribution and then project the resulting point onto the surface of the hypersphere.²³

The non-local sampling consists of a modified Wolff cluster update, where we add to the standard Wolff algorithm²² a cluster acceptance probability to account for the onsite energy terms in H_2 in Eq. (4). As expected, the non-local sampling provides notable efficiency gain (which becomes more significant as the temperature decreases) and also helps to prevent the ergodicity loss that can occur at low temperatures. We note that the non-local cluster sampling described above is not possible when $\lambda \neq 1$ due to the anisotropic coupling that results between the hyperplanes corresponding to Ψ and Φ_μ ($\mu = x, y$). However, at moderate temperatures, it is still possible to obtain reasonable results with $\lambda \neq 1$ using only local sampling.

Using such updates, a Monte Carlo procedure is capable of calculating all standard estimators, such as the energy and magnetization. In order to compute $R(T)$ in Eq. (1), one needs to access two specific quantities, namely the linear-order diamagnetic susceptibility M/B , and the correlation length ξ_{cdw} of CDW correlations. We begin by describing our procedure for the latter. We perform Monte Carlo simulations to compute the CDW correlation function

$$C_{\Phi_x}(\mathbf{r}_i - \mathbf{r}_j) = \left\langle \sum_{\alpha=3}^4 n_{i\alpha} n_{j\alpha} \right\rangle \quad (18)$$

on an $L \times L$ lattice, with periodic boundary conditions (in order to minimize potential edge effects). We then calculate the structure factor

$$S_{\Phi_x}(\mathbf{q}) = \sum_{\mathbf{r}} C_{\Phi_x}(\mathbf{r}) \cos(\mathbf{q} \cdot \mathbf{r}) \quad (19)$$

with $\mathbf{q} = q_x \hat{x}$, and compare various methods for extracting ξ_{cdw} . The first such method involves a least-squares fit of $S_{\Phi_x}(q_x)$ to a shifted Lorentzian function,

$$A (q_x^2 + 1/\xi^2)^{-1} + c. \quad (20)$$

We add the shift c to the Lorentzian fitting function to account for the effects of the missing short-wavelength degrees of freedom, which are significant here since ξ_{cdw} is of the order of the lattice spacing a . The second method, as described in Ref. 24, is obtained by assuming the Ornstein-Zernike form for the correlation function and subsequently calculating ξ_{cdw} from

$$\xi_{\text{cdw}} = \frac{L}{2\pi} \sqrt{\left(\frac{8d}{(1+d)(3+d)} \right) \left(\frac{S_{\Phi_x}(0)}{S_{\Phi_x}(\frac{2\pi}{La} \hat{x})} - 1 \right)}. \quad (21)$$

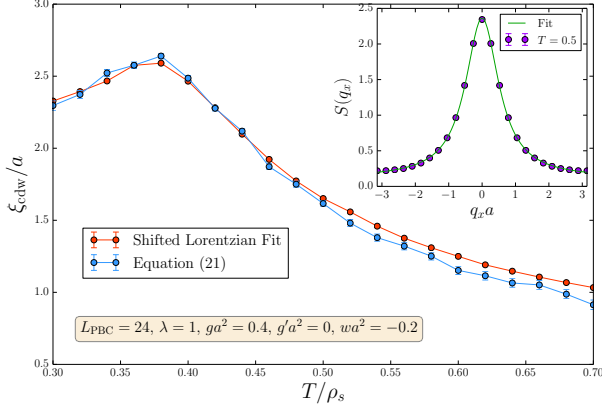


FIG. 2. The CDW correlation length ξ_{cdw} extracted from Monte Carlo simulations. We illustrate two different methods for extracting the correlation length for a representative set of parameters. The first method fits the structure factor $S(q_x)$ to the shifted Lorentzian function of Eq. (20) for each T , as illustrated in the inset for $T = 0.5$. Error bars come from the covariance matrix of the least-squares fit. The second method is to calculate ξ_{cdw} from Eq. (21), with error bars corresponding to the statistical Monte Carlo error.

Results for ξ_{cdw} vs. T are shown in Figure 2 for $L = 24$. Note that careful finite-size scaling analysis concludes that the data for ξ_{cdw} extracted through these procedures is converged by lattice size $L = 24$ for the model parameters studied in this paper.

Next, we also use Monte Carlo methods to calculate the linear-order diamagnetic susceptibility, M/B . For these calculations, we write Eq. (17) in terms of the coordinates n_{i1} and n_{i2} as

$$\begin{aligned} \chi_d \equiv \frac{M}{B} = & -\frac{\rho_s}{4L^2 s} \sum_i \sum_{u=+\hat{x}a, +\hat{y}a} (\epsilon_{\alpha\beta} r_{i\alpha} u_\beta)^2 \\ & \times \langle n_{i1} n_{i+u,1} + n_{i2} n_{i+u,2} \rangle_0 \\ & + \frac{\rho_s^2}{4TL^2 s} \left\langle \left[\sum_i \sum_{u=+\hat{x}a, +\hat{y}a} (\epsilon_{\alpha\beta} r_{i\alpha} u_\beta) \right. \right. \\ & \left. \left. \times (n_{i1} n_{i+u,2} - n_{i2} n_{i+u,1}) \right]^2 \right\rangle_0. \end{aligned} \quad (22)$$

These simulations are performed separately from those for calculating ξ_{cdw} since, as described in Section II, our method for calculating M/B requires a lattice with open boundary conditions. Results for the diamagnetic susceptibility are shown for various lattice lengths L for a given set of parameters λ , g , g' and w in Fig. 3. For $T > T_c$, $\chi_d = M/B$ converges well to a limiting value as $L \rightarrow \infty$. We discuss the situation below the Kosterlitz-Thouless transition in Appendix B: there we show that $s\chi_d = -0.0351\rho_s^R(La)^2$, where ρ_s^R is the renormalized stiffness; the divergence as $L \rightarrow \infty$ is a manifestation of the Meissner effect.

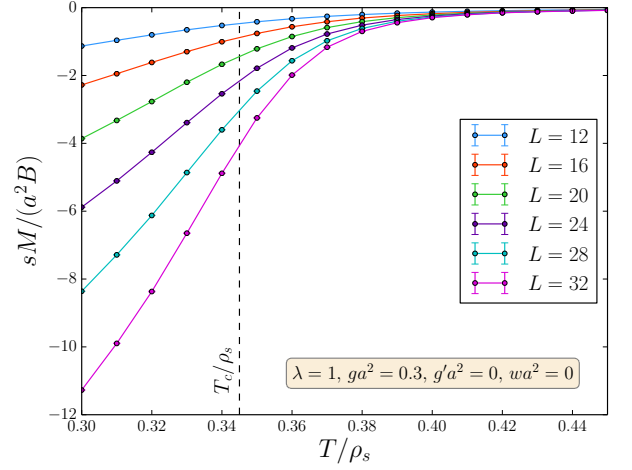


FIG. 3. Monte Carlo calculations of the linear diamagnetic susceptibility M/B . We plot $sM/(a^2 B)$ for a representative set of parameters and various L , with M/B calculated from Eq. (22) in a Monte Carlo simulation on a system with open boundary conditions. The dashed line is the location of the Kosterlitz-Thouless transition.

IV. RESULTS

Using our Monte Carlo calculations of the CDW correlation length and linear diamagnetic susceptibility in the model described above, we are ready to calculate the dimensionless ratio $R(T)$ to compare to experiment. In order to calculate the experimental quantity, we write the measurements of the diamagnetic susceptibility in the form, following Ref. 4,

$$M(T) \equiv -\left(\frac{2e}{\hbar}\right)^2 \frac{TB}{12\pi s} \xi_{ab}^2(T) \quad (23)$$

where we take Eq. (23) as the *definition* of the length $\xi_{ab}(T)$, which is determined from torque magnetometry experiments on underdoped $\text{YBa}_2\text{Cu}_3\text{O}_{6.5}$ with $T_c = 57 \text{ K}$.²⁵ Then the experimental value of the ratio $R(T)$ is simply

$$R(T) = -\left(\frac{\xi_{ab}(T)}{\xi_{\text{cdw}}^{\text{Xray}}(T)}\right)^2 \quad (24)$$

where $\xi_{\text{cdw}}^{\text{Xray}}(T)$ is the correlation length of the charge order determined from X-ray scattering experiments on oxygen-disordered $\text{YBa}_2\text{Cu}_3\text{O}_{6.67}$ with $T_c = 65.5 \text{ K}$.¹² To extract this correlation length, we first subtract the X-ray fluorescence background using a measurement at 160 K and then fit the resulting profile using a Lorentzian function. Results for $\xi_{\text{cdw}}^{\text{Xray}}(T)$ vs. T , as well as this fitting procedure, are illustrated in Figure 4.

In order to compare these results to our Monte Carlo calculations of the dimensionless ratio in Eq. (1), we must first determine the value of ρ_s for each set of parameters

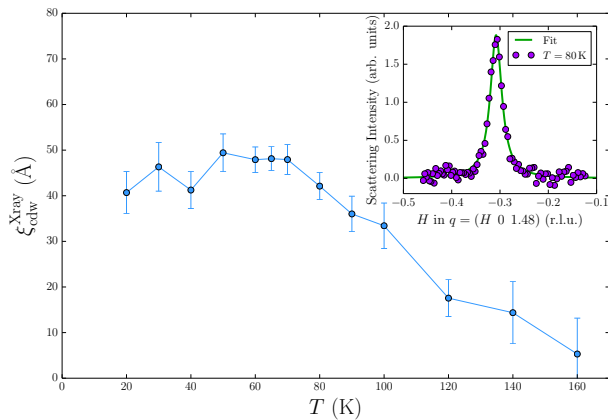


FIG. 4. The CDW correlation length $\xi_{\text{cdw}}^{\text{Xray}}$ extracted from X-ray scattering experiments¹² on $\text{YBa}_2\text{Cu}_3\text{O}_{6.67}$ as a function of T . $\xi_{\text{cdw}}^{\text{Xray}}(T)$ is extracted from Lorentzian fits to background-subtracted X-ray scattering data. The inset illustrates this fit for data at $T = 80$ K. The error bars reflect the statistical uncertainty in the fit and additional uncertainty due to the background subtraction.

λ , ga^2 , $g'a^2$ and wa^2 in our model. To do this, we use the procedure of Ref. 17 to compute the structure factor in Eq (19) with $\mathbf{q} = 0$. We compare our results for $S_{\Phi_x}(\mathbf{q} = 0)$ with CDW scattering intensities from X-ray scattering experiments and determine ρ_s (as well as the vertical scaling factor for the Monte Carlo data) by requiring that the curves match in the vicinity of the peak. This procedure is illustrated in Fig. 5.

In Figure 6, we compare our Monte Carlo simulations of the dimensionless ratio $R(T)$ (after determining ρ_s as explained in Fig. 5) against the corresponding experimental values defined in Eq. (24) with no additional fitting parameters. The close correspondence between theory and experiment in both the absolute value and T dependence of $R(T)$ is evidence that our model has captured significant aspects of the underlying physics. However, the theoretical values of $R(T)$ are consistently smaller than the experimental values; this discrepancy could be due to the different samples used for the diamagnetism and charge order measurements in computing $R(T)$, or due to the limitations of our model, which are discussed in Section V.

V. CONCLUSIONS

This paper has presented Monte Carlo results on an effective classical model of competing superconducting and density wave orders in the underdoped cuprates. Previous work¹⁷ has shown that the model can provide an excellent fit to the temperature dependence of the structure factor of the density wave correlations in the pseudogap regime, as measured by X-ray scattering experiments. The present paper applied the same model to superconducting fluctuations as detected by diamagnetism

measurements. We characterized the strength of the diamagnetism by a dimensionless number $R(T)$, whose value is directly measurable in experiments, and which can also be conveniently computed in our Monte Carlo simulations. We found that the same set of fitting parameters used to describe X-ray scattering also successfully capture the numerical value and variation with T of $R(T)$.

However, the present classical model does omit some significant aspects of the physics. It does not include the effects of random field disorder acting on the charge order:²⁶ we expect this to be important for enhancing the static component of the charge order at low T , where there are deviations between our theory and the X-ray results. Interlayer couplings have also been omitted, and these will reduce the strength of superconducting fluctuations above T_c , and possibly provide the needed correction to the theoretical value of $R(T)$. Our model also does not make explicit reference to the fermionic degrees of freedom, but we believe these are properly accounted for by our effective theory at the T values of interest in the X-ray structure factor and the diamagnetism measurements.

With the improvements of our model just described, and precise experimental measurements of both diamagnetism and charge order correlations on the same sample, we believe the prospects are bright for a precise quantitative theory of the pseudogap regime of the cuprate superconductors.

ACKNOWLEDGMENTS

We thank D. Chowdhury, J. R. Cooper, S. Kivelson, M. Gingras, Laimei Nie and L. Taillefer for useful discussions. This research was supported by the NSF under Grant DMR-1103860, the Natural Sciences and Engineering Research Council of Canada, the Perimeter Institute for Theoretical Physics, the John Templeton Foundation, and the Canada Research Chair program. Research at Perimeter Institute is supported by the Government of Canada through Industry Canada and by the Province of Ontario through the Ministry of Research and Innovation.

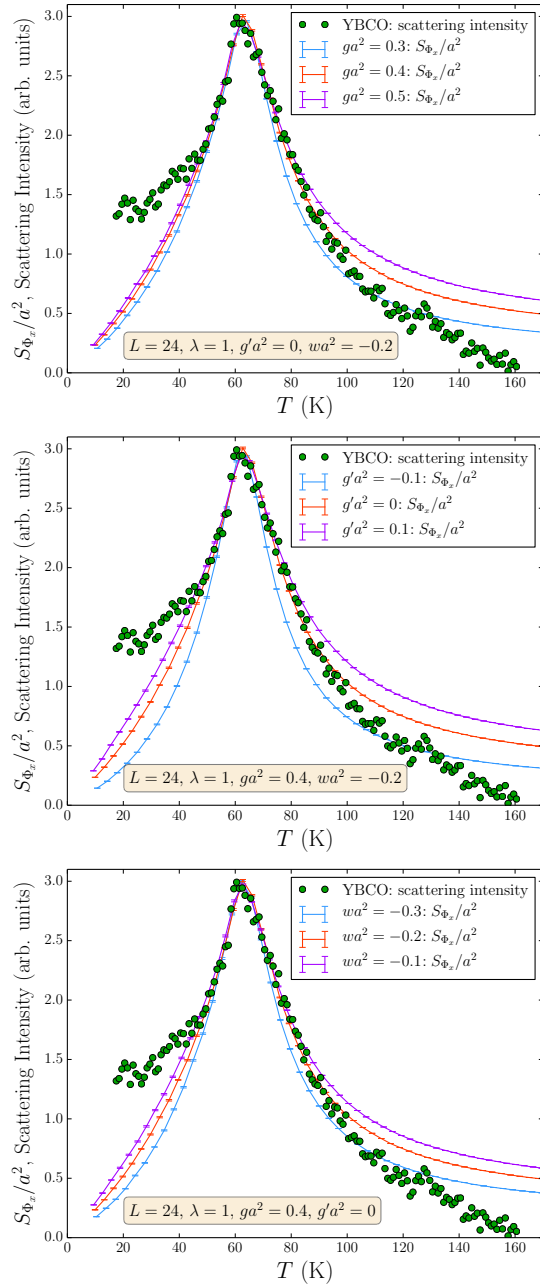


FIG. 5. Comparison of S_{Φ_x} calculated in Monte Carlo simulations to X-ray data from CDW scattering experiments¹² on $\text{YBa}_2\text{Cu}_3\text{O}_{6.67}$. We illustrate results that demonstrate the effects of varying g (top), g' (middle) and w (bottom) in our model. Note that, following the procedure of Ref. 17, there are two fitting parameters for each set of parameters λ , ga^2 , $g'a^2$ and wa^2 : the value of ρ_s as well as the vertical scaling factor were both adjusted to make the Monte Carlo and experimental curves match in the vicinity of the peak.

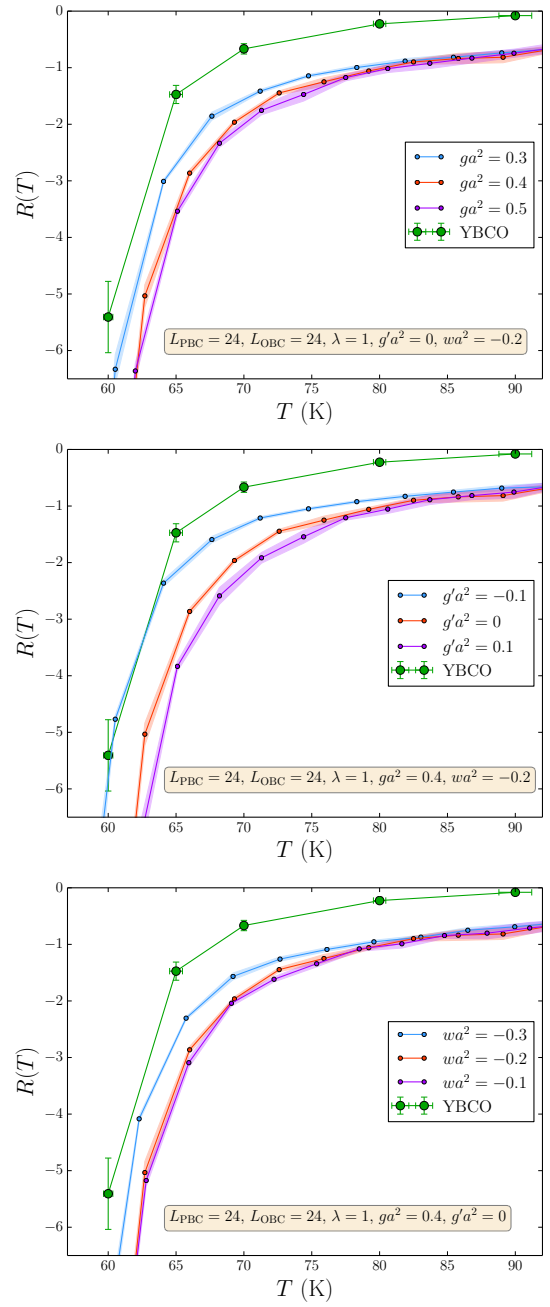


FIG. 6. Comparison of $R(T)$ calculated in Monte Carlo simulations to data from X-ray scattering experiments¹² and torque magnetometry experiments⁴ on YBCO. We illustrate results for the same parameter sets as in Figure 5. For each set of parameters λ , ga^2 , $g'a^2$ and wa^2 , the rescaling factor for the Monte Carlo data along the T -axis is determined from the S_{Φ_x} vs. T fit. The shading for $R(T)$ accounts for statistical Monte Carlo errors as well as the uncertainty in the method for extracting ξ_{cdw} (see Figure 2).

Appendix A: Gaussian theory

As alluded to in Section II, we tested our Monte Carlo method for calculating the linear-order diamagnetic susceptibility on a simple Gaussian theory for the SC order

$$\begin{aligned}
 H &= \frac{\rho_s}{2} \sum_{\langle ij \rangle} |\Psi_i - \Psi_j|^2 + \frac{\rho_s}{2} \sum_i \bar{\sigma} |\Psi_i|^2 \\
 &= \frac{\rho_s}{2} \left[\sum_i (Z_i + \bar{\sigma}) |\Psi_i|^2 - \sum_{i,u} \Psi_i^* \Psi_{i+u} \right] \\
 &\equiv \frac{\rho_s}{2} \sum_{i,j} \Psi_i^* \mathcal{M}_{i,j} \Psi_j, \quad (\text{A1})
 \end{aligned}$$

while ignoring all constraints, interactions, and the CDW components. Here $\mathcal{M}_{i,j}$ is a matrix defined by the expressions above. This appendix drops factors of the inter-layer spacing s , and sets the lattice spacing $a = 1$. Then

$$\begin{aligned}
 \frac{M}{BT} &= -\frac{1}{4L^2} \sum_{i,u} (\epsilon_{\alpha\beta} r_{i\alpha} u_\beta)^2 \mathcal{M}_{i,i+u}^{-1} \\
 &+ \frac{1}{4L^2} \sum_{i,u} \sum_{j,u'} (\epsilon_{\alpha\beta} r_{i\alpha} u_\beta) (\epsilon_{\gamma\delta} r_{j\gamma} u'_\delta) \mathcal{M}_{i,j}^{-1} \mathcal{M}_{j+u',i+u}^{-1}. \quad (\text{A2})
 \end{aligned}$$

Note that the right-hand-side is independent of ρ_s and T : this is a special feature of the Gaussian theory. The exact answer for the Gaussian theory in the limit $L \rightarrow \infty$ is¹⁷

$$\begin{aligned}
 \frac{M}{BT} &= -\int \frac{d^2 k}{4\pi^2} \frac{8 \sin^2(k_x) \sin^2(k_y)}{(4 - 2 \cos(k_x) - 2 \cos(k_y) + \bar{\sigma})^4} \quad (\text{A3}) \\
 &= -\frac{1}{12\pi\bar{\sigma}} \quad \text{as } \bar{\sigma} \rightarrow 0. \quad (\text{A4})
 \end{aligned}$$

We compare the above expressions with our Monte Carlo results in Table I. The excellent agreement between the theory and the Monte Carlo results is strong evidence that our simulations have converged to the thermodynamic diamagnetic susceptibility.

Appendix B: Superconducting phase

For the superconducting phase we use the simple action

$$H_{sf} = \frac{\rho_s^R}{4} \sum_{i,u} (\theta_i - \theta_{i+u} - A_{iu})^2 + \frac{\rho_s^R m_\theta^2}{2} \sum_i \theta_i^2, \quad (\text{B1})$$

where ρ_s^R is the renormalized phase stiffness, and m_θ is a small mass added as an infrared regulator; the final result for the magnetization will have a smooth limit as $m_\theta \rightarrow 0$. So the current flowing along link iu is

$$\mathbf{J}_{iu} = \mathbf{u} \rho_s^R (\theta_i - \theta_{i+u} - A_{iu}). \quad (\text{B2})$$

$\bar{\sigma}$	L	$M/(BT)$ Eq. (A2)	$M/(BT)$ Eq. (A3)	Monte Carlo
1	5	-0.011490		-0.01149(2)
1	10	-0.011206		-0.01124(5)
1	20	-0.011108		-0.0110(2)
1	40	-0.011064		-0.0113(6)
1	80	-0.011043		-0.010(2)
1	∞	-0.011028(3)	-0.011024	-0.0108(4)
0.5	5	-0.038279		-0.03826(2)
0.5	10	-0.034226		-0.03426(5)
0.5	20	-0.032718		-0.0326(4)
0.5	40	-0.032004		-0.031(1)
0.5	80	-0.031656		-0.026(4)
0.5	∞	-0.03139(4)	-0.031315	-0.0308(9)
0.1	5	-0.420271		-0.404(4)
0.1	10	-0.322547		-0.320(2)
0.1	20	-0.268920		-0.275(6)
0.1	40	-0.247611		-0.24(1)
0.1	80	-0.237534		-0.18(3)
0.1	∞	-0.224(3)	-0.227827	-0.22(1)

TABLE I. Magnetization for the Gaussian theory H in Eq. (A1). The extrapolation to $L = \infty$ in the third and fifth columns is performed by a least-squares fit to a quadratic polynomial of $1/L$, and the error bars for $L = \infty$ come from the covariance matrix of the least-squares fit. The Monte Carlo data in the fifth column was taken at $T = 0.6$, although we also checked that the Monte Carlo results for $M/(BT)$ are independent of T .

We can then write the total magnetic moment divided by the volume as

$$M = \frac{\rho_s^R}{4L^2 a^2 s} \sum_{i,u} \epsilon_{\alpha\beta} r_{i\alpha} u_\beta \langle \theta_i - \theta_{i+u} - A_{iu} \rangle. \quad (\text{B3})$$

Again, we expand M to first order in B and obtain

$$\begin{aligned}
 \frac{M}{B} &= -\frac{\rho_s^R}{8L^2 a^2 s} \sum_{i,u} (\epsilon_{\alpha\beta} r_{i\alpha} u_\beta)^2 \\
 &+ \frac{(\rho_s^R)^2}{16TL^2 a^2 s} \sum_{i,u} \sum_{j,u'} (\epsilon_{\alpha\beta} r_{i\alpha} u_\beta) (\epsilon_{\gamma\delta} r_{j\gamma} u'_\delta) \\
 &\quad \times \left\langle (\theta_i - \theta_{i+u})(\theta_j - \theta_{j+u'}) \right\rangle_0, \quad (\text{B4})
 \end{aligned}$$

where the subscript indicates that this average is to be evaluated under H_{sf} at zero field. If we write the field-

independent part of H_{sf} as

$$\begin{aligned} H_{sf}^0 &= \frac{\rho_s^R}{4} \sum_{i,u} (\theta_i - \theta_{i+u})^2 + \frac{\rho_s^R m_\theta^2}{2} \sum_i \theta_i^2 \\ &\equiv \frac{\rho_s^R}{2} \sum_{i,j} \theta_i \mathcal{N}_{i,j} \theta_j, \end{aligned} \quad (\text{B5})$$

then

$$\begin{aligned} \frac{sM}{B\rho_s^R} &= -\frac{1}{8L^2 a^2} \sum_{i,u} (\epsilon_{\alpha\beta} r_{i\alpha} u_\beta)^2 \\ &\quad + \frac{1}{16L^2 a^2} \sum_{i,u} \sum_{j,u'} (\epsilon_{\alpha\beta} r_{i\alpha} u_\beta) (\epsilon_{\gamma\delta} r_{j\gamma} u'_\delta) \\ &\quad \times (\mathcal{N}_{i,j}^{-1} + \mathcal{N}_{i+u,j+u'}^{-1} - \mathcal{N}_{i+u,j}^{-1} - \mathcal{N}_{i,j+u'}^{-1}). \end{aligned} \quad (\text{B6})$$

We evaluate this expression numerically, and the $L \rightarrow \infty$ results are in precise agreement with the analytic results described below.

For an analytic expansion in the continuum limit, we can express the magnetization in terms of the θ propagator $G_\theta(\mathbf{r}, \mathbf{r}')$. The propagator is conveniently expressed in terms of the eigenmodes of the Laplacian with Neumann (zero current) boundary conditions as

$$\frac{\rho_s^R}{T} G_\theta(\mathbf{r}, \mathbf{r}') = \sum_{m,n=0}^{\infty} \frac{\phi_{m,n}(\mathbf{r}) \phi_{m,n}(\mathbf{r}')}{(m^2 + n^2) \pi^2 / L^2 + m_\theta^2}, \quad (\text{B7})$$

where the eigenmodes are

$$\phi_{m,n}(\mathbf{r}) = \begin{cases} 1/L, & m = n = 0 \\ (\sqrt{2}/L) \cos(m\pi(x/L - 1/2)), & n = 0, m \neq 0 \\ (\sqrt{2}/L) \cos(n\pi(y/L - 1/2)), & m = 0, n \neq 0 \\ (2/L) \cos(m\pi(x/L - 1/2)) \\ \quad \times \cos(n\pi(y/L - 1/2)), & n \neq 0, m \neq 0. \end{cases} \quad (\text{B8})$$

Then, the continuum limit of Eq. (B6) at $m_\theta = 0$ is

$$\begin{aligned} \frac{sM}{B\rho_s^R a^2} &= -\frac{1}{4L^2} \int_{-L/2}^{L/2} dx \int_{-L/2}^{L/2} dy (x^2 + y^2) \\ &\quad + \frac{\rho_s^R}{4TL^2} \int_{-L/2}^{L/2} dx \int_{-L/2}^{L/2} dy \int_{-L/2}^{L/2} dx' \int_{-L/2}^{L/2} dy' \\ &\quad \left[(\mathbf{r} \times \nabla_{\mathbf{r}})(\mathbf{r}' \times \nabla_{\mathbf{r}'}) G_\theta(\mathbf{r}, \mathbf{r}') \right] \\ &= -\frac{L^2}{24} + \frac{L^2}{\pi^6} \sum_{m,n=1}^{\infty} (-1 + (-1)^m)^2 (-1 + (-1)^n)^2 \\ &\quad \times \frac{(m^2 - n^2)^2}{m^4 n^4 (m^2 + n^2)} \\ &= -0.03514425 L^2. \end{aligned} \quad (\text{B9})$$

The numerical values of Eq. (B6) agree very well with the above result. The linear diamagnetic susceptibility of a two-dimensional superconductor in an $La \times La$ square geometry thus diverges as $-0.03514425 \rho_s^R (La)^2$ in the limit of large L ; this is, of course, a manifestation of the Meissner effect.

¹ Y. Wang *et al.*, Phys. Rev. Lett. **95**, 247002 (2005).

² Lu Li *et al.*, Nat. Phys. **3**, 311 (2007).

³ Lu Li *et al.*, Phys. Rev. B **81**, 054510 (2010).

⁴ I. Kokanović *et al.*, Phys. Rev. B **88**, 060505(R) (2013).

⁵ A. Larkin and A. Varlamov, *Theory of Fluctuations in Superconductors* (Clarendon, Oxford, U.K., 2005).

⁶ V. Oganessian, D. A. Huse, and S. L. Sondhi, Phys. Rev. B **73**, 094503 (2006).

⁷ D. Podolsky, S. Raghu, and A. Vishwanath, Phys. Rev. Lett. **99**, 117004 (2007).

⁸ K. Sarkar, S. Banerjee, S. Mukerjee, and T. V. Ramakrishnan, arXiv:1309.3776.

⁹ G. Ghiringhelli *et al.*, Science **337**, 821 (2012).

¹⁰ J. Chang *et al.*, Nature Phys. **8**, 871 (2012).

¹¹ A. J. Achkar *et al.*, Phys. Rev. Lett. **109**, 167001 (2012).

¹² A. J. Achkar *et al.*, arXiv:1312.6630.

¹³ R. Comin *et al.*, Science **343**, 390 (2014).

¹⁴ R. Comin *et al.*, arXiv:1402.5415.

¹⁵ E.H. da Silva Neto *et al.*, Science **343**, 393 (2014).

¹⁶ J. E. Hoffman *et al.*, Science **295**, 466 (2002).

¹⁷ L. E. Hayward, D. G. Hawthorn, R. G. Melko, and S. Sachdev, Science **343**, 1336 (2014).

¹⁸ C. Ebner and D. Stroud, Phys. Rev. B **31**, 165 (1985).

¹⁹ N. Metropolis, A. W. Rosenbluth, M. N. Rosenbluth, A. H. Teller and E. Teller, J. Chem. Phys. **21**, 1087 (1953).

²⁰ W.K. Hastings, Biometrika **57**, 97 (1970).

²¹ M. E. Newman and G. T. Barkema, *Monte Carlo Methods in Statistical Physics* (Oxford University Press, 1999).

²² U. Wolff, Phys. Rev. Lett. **62**, 361 (1989).

²³ G. Marsaglia, Ann. Math. Stat. **43** 645 (1972).

²⁴ A. Sandvik, arXiv:1101.3281.

²⁵ We thank J. R. Cooper for providing us the values of $\xi_{ab}(T)$, defined as in Eq. (23), from Ref. 4.

²⁶ Laimei Nie, G. Tarjus, and S. A. Kivelson, PNAS **111**, 7980 (2014).